

ULUSLARARASI 3B YAZICI TEKNOLOJİLERİ
VE DİJİTAL ENDÜSTRİ DERGİSİ

INTERNATIONAL JOURNAL OF 3D PRINTING
TECHNOLOGIES AND DIGITAL INDUSTRY

ISSN:2602-3350 (Online)

URL: <https://dergipark.org.tr/ij3dptdi>

APPLICATION OF TOPOLOGY OPTIMIZATION ON A 3D-PRINTED SHELF BRACKET

Yazarlar (Authors): Berker Özün Fenni ^{ID}*, Ersin Eken ^{ID}, Hüseyin Kaygısız ^{ID}


Bu makaleye şu şekilde atıfta bulunabilirsiniz (To cite to this article): Fenni B. Ö., Eken E., Kaygısız H., "Application of Topology Optimization on A 3d-Printed Shelf Bracket" Int. J. of 3D Printing Tech. Dig. Ind., 8(1): 32-45, (2024).

DOI: 10.46519/ij3dptdi.1331696

Araştırma Makale/ Research Article

Erişim Linki: (To link to this article): <https://dergipark.org.tr/en/pub/ij3dptdi/archive>

APPLICATION OF TOPOLOGY OPTIMIZATION ON A 3D-PRINTED SHELF BRACKET

Berker Özün Fenni^a , Ersin Eken^a , Hüseyin Kaygısız^b 

^aIstanbul Gedik University, Engineering Faculty, Mechanical Engineering Department, TURKEY

^bIstanbul Gedik University, Vocational School, Machinery Programme, TURKEY

*Sorumlu Yazar: berker.ozun@hotmail.com

(Received: 24.07.23; Revised: 24.11.23; Accepted: 31.01.24)

ABSTRACT

In this study, the topology optimization approach was adopted to reduce the material used in manufacturing. Specifically, the mass optimization technique was deemed suitable. Mass optimization eliminates the parts that don't affect a bracket's overall strength while under load, resulting in weight reduction and material savings. Two shelf brackets were designed to test this theory and were subjected to mass optimization. A static structural analysis of this optimized model was carried out to confirm the optimization findings. These designs were then manufactured using the 3D-printing process. The yield points were next determined by performing a uniaxial tensile test on the shelf brackets. The outcome of the tests was subsequently compared with the simulation results, and a cost analysis model was created as an output. Ultimately, a reduction of 70% in mass was achieved with acceptable structural strength. In related optimization studies, the connecting part of an unmanned aerial vehicle's landing gear has been optimized resulting in fuel savings. The theory that topology optimization may be used to make both light and stiff parts at the same time has been proven by the results of this research as well as other studies that have been done on the same topic.

Keywords: Topology optimization, finite element analysis, 3D-printing, CAD.

1. INTRODUCTION

With the rapid advancement of the manufacturing industry, the need for lightweight and durable parts has increased exponentially. To accommodate this, research has been carried out to find ways to make goods faster at a lower cost. Therefore, developing and manufacturing these parts has become increasingly important with time.

In industries such as automotive, there is a continuing need for lighter and more durable parts. In order to sell more cars, the manufacturers always competed for better fuel efficiency. As the vehicles get lighter, it will result in a reduction in fuel consumption as well. Consequently, mass optimization is a possible approach to reducing fuel consumption in vehicles [1].

As a result, the finite element analysis (FEA) was created to address these problems in engineering. This matrix-based method has then enabled the use of structural analysis methods in engineering. In the years that followed, the FEA approach was improved, and methods for structure optimization were introduced.

Structural optimization, also known as topology optimization (TO), reduces the amount of material used by only assigning it to the parts' load-bearing regions and eliminating it from the regions that have the least effect on the design's strength and natural frequency. Numerous TO techniques are available nowadays that may be used according to the intended use and compatibility of the design [2].

The FEA is a numerical method used to derive approximate solutions for various engineering problems. This method allows for analyzing stress, heat transfer, fluid mechanics, and electromagnetism problems that exhibit time dependence, independence, linearity, and nonlinearity. According to Moaveni [3], simplification techniques, such as iteration and approximate mathematical methods, have solved complex engineering problems typically addressed by applying mathematical formulas and expressions.

Moaveni [3] asserts that Courant is widely recognized as the individual who pioneered the finite element method in 1943. The next significant advancement in applying FEA commenced during the 1950s when Boeing incorporated triangular tension elements to model aircraft wings.

In 1967, Zienkiewicz and Chung published the first work in this field. Then, in the late 1960s, MSC created the first piece of FEA software, NASTRAN. Subsequently, the ANSYS software was developed in 1971. ANSYS can perform various types of analysis, including static, dynamic, heat transfer, fluid mechanics, and electromagnetism analyses [4]. Numerous software applications for FEA have been developed over time.

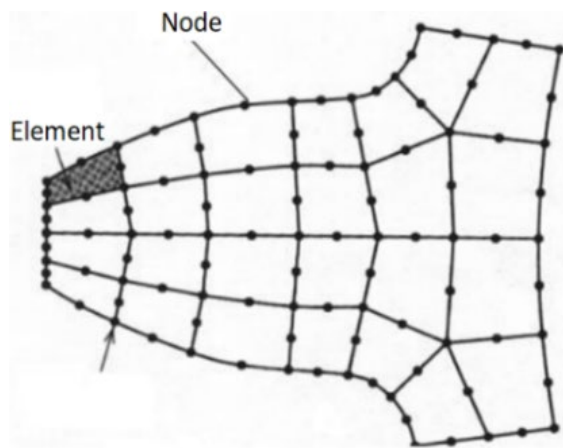


Figure 1. Depiction of elements and nodes in FEA [5].

In order to perform structural analysis, the model must be meshed. The process of dividing the model into discrete elements and nodes is called meshing, as seen in Fig. 1. As the quantity of elements increases, the number of iterations will correspondingly increase. This progressive increase in iterations leads to a convergence towards the actual result, thereby enabling the determination of a more accurate and refined outcome.

Upon the completion of meshing, it is vital to assign mechanical properties and material characteristics to the model. Typically, these characteristics encompass Young's modulus, which pertains to elasticity, and Poisson's ratio. Once the process of mesh modeling has been finalized, boundary conditions and loads are subsequently imposed on the elements and the nodal points. The structural analysis can begin after these prerequisites are met.

Structural analysis may be classified into two categories: dynamic and static. This study involves the execution of linear static analysis. Stress, shear stress (von Mises stress), principal forces (principal stresses), the factor of safety (FoS), and strain or deformation are some of the things that are looked at in the analyses. The desired values may be determined by applying these criteria to the solution [6].

After the analysis has been completed, structural optimization can begin. TO is a technique for structural optimization that has been developed within the realm of FEA. This method is widely employed across various industries, including automotive, aviation, and construction. TO aims to achieve the most efficient allocation of material within specified boundary conditions. Regions that do not significantly impact a part's overall strength and natural frequency when subjected to a load are eliminated through conditions that reduce mass or volume. By employing this method, resources are conserved, achieving optimal structural rigidity and the lightest possible design.

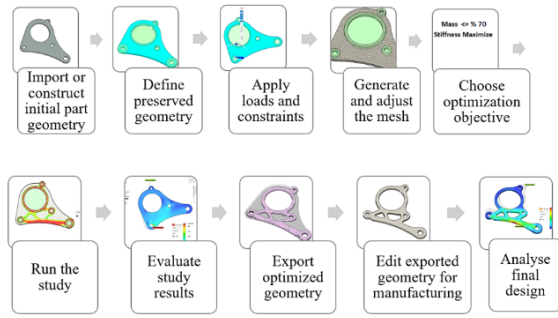


Figure 2. Shape optimization flow chart [7].

As illustrated in Fig. 2: The process begins with the creation of a model. Then the file is submitted to the analysis software, where critical parts that are not intended to be removed are excluded. Next, load allocation and boundary conditions are put in, generating the model's mesh. Subsequently, the optimization objective is put in. Then, a new analysis is performed on the optimized model to validate the analysis findings.

There are numerous studies in the literature that demonstrate the success of mass optimization. One of these is a biomedical paper by Ege and Küçük [8]. According to Ege and Küçük, reducing the weight by utilizing particle swarm optimization on a robotic-type above-knee prosthesis may enhance battery life. Several optimizations were carried out to determine the best outcome. These optimized specimens were then manufactured using a 3D printer and tested with a DC motor. The specimen with 60% infill rate yielded the best results, successfully increasing the battery life of the robotic prosthesis by 51%, or 1.89 hours while maintaining acceptable structural rigidity.

The formulation for mass optimization is as follows:

$$(K - \omega^2 M)u = f \quad (1)$$

'K' is the global stiffness matrix, so the global mass matrix 'M' may also be given as:

$$K = \sum_{i=1}^{N_e} \int_{\Omega} K^{(i)} d\Omega \quad (2)$$

$$M = \sum_{i=1}^{N_e} \int_{\Omega} M^{(i)} d\Omega \quad (3)$$

The element stiffness matrix, denoted as ' $K^{(i)}$ ' and the element mass matrix, shown as ' $M^{(i)}$ ', are matrices used to analyze a given region ' Ω '. The variable 'i' represents the specific element being considered. The angular frequency is represented by ' ω ', the node load vector by 'f', and the vector displacements by 'u'. Additionally, ' N_e ' represents the total elements [9].

The analysis incorporates structural damping as a complex element stiffness matrix to guarantee a solution to Eq. 1 across all natural frequencies.

$$K^e = K_0^i (1 + \eta(\omega)), \begin{cases} \eta = \hat{\eta} & \omega > 0 \\ \eta = 0 & \omega = 0, \end{cases} \quad (4)$$

In order to differentiate the static stiffness matrix of the undamped system, the number '0' is added to the subscript. Additionally, ' $\hat{\eta}$ ' represents the structural loss factor. To address the given static equation, the value of ' $\omega = 0$ ' is selected and denoted as ' u_{static} '. The design variables involve the presence or exclusion of material in each element. Consequently, the stiffness, mass matrices, and displacements depend on these design variables. External load is assumed to be independent of design variables [9].

The shape that results from optimization will be intricate in nature. As a result, the utilization of traditional manufacturing procedures for these parts may be challenging. Consequently, different manufacturing methods must be considered.

Casting is one of the processes described. However, the strength of cast parts is not always satisfactory. Furthermore, for each new part, a new mold must be made, vastly increasing the upfront cost of casting. As a result, another manufacturing method must be considered. Consequently, additive manufacturing (AM) was introduced. Later, these intricate geometries started being produced cheaper using AM [10].

Fused deposition modeling (FDM), commonly referred to as 3D-printing, has significantly transformed the manufacturing sector. This method enables the rapid and cost-effective production of structures with intricate geometries, surpassing the capabilities of

conventional manufacturing techniques. The manufacturing of polymeric materials, such as ABS and PLA, has been prevalent in the initial stages of this process. However, recent technological advancements have enabled the production of metallic components [11,12]

Wohler and Gornet [13] assert that the initial sample of AM was created by 3D Systems in 1987, known as stereolithography. The aforementioned procedure is executed through the utilization of the curing of photosensitive ultraviolet (UV) liquid polymers or photopolymer resins. The acronym STL is derived from the nomenclature of the stereolithography technique employed in this additive manufacturing process.

In 1991, FDM was developed. This system is the precursor to contemporary 3D-printing machines that employ filaments. The process involves the introduction of polymer filaments into the hot nozzle and extruder, which are deposited in a layered manner on the bed to fabricate a three-dimensional model, which may be seen in Fig. 3 [13].

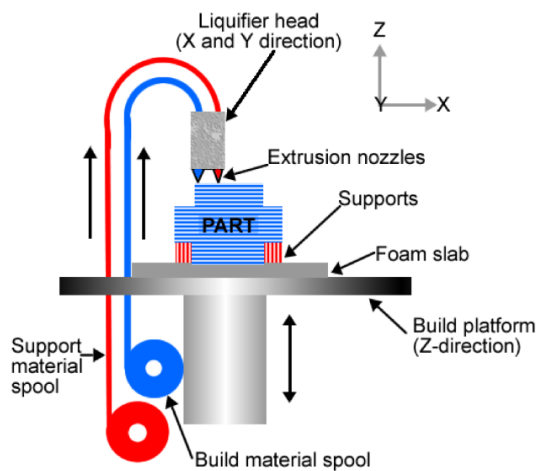


Figure 3. FDM printing machine schematic [14].

The strength of 3D-printed parts is influenced by various factors, including the choice of filaments and parameters such as layer thickness, extrusion temperature, infill rate, printing speed, printing angle, and printing direction [15].

Regarding the variation in strength concerning the extrusion angle, Gonabadi et al. [16] stated that the tensile strength decreases as the extrusion angle approaches 90° . Conversely, the strength increases as the angle decreases as seen in Fig. 4, graph a.

As for the printing direction, the tensile strength of a 3D-printed part is typically weaker in the deposition direction due to the inherent characteristics of the deposition process. When a part is printed along the "Z" axis, it exhibits reduced strength in that particular direction. The material in question is referred to as transversely isotropic, as Gonabadi et al. [16] indicated (Fig. 4, graph c).

Delaminating these materials within their walls are comparatively easier than attempting to crush them in the opposite direction.

The influence of the infill pattern on the tensile strength of 3D-printed components has been observed in the research conducted by Gonabadi et al. [16]. The study examined four distinct printing patterns. Based on the examination of the test results, it may be observed that both triangle and square patterns exhibited comparable characteristics. The patterns of triangles and squares exhibited the lowest strain levels, as depicted in Fig. 3 (graph b).

The infill density may also influence the tensile strength of 3D-printed parts. According to the findings of Gonabadi et al. [16], it can be observed that an increase in infill density leads to an equal rise in tensile strength.

In conclusion, the stress-strain curves depicted in Fig. 4 illustrate the influence of various parameters on the tensile strength of 3D-printed components. In light of this information, the following parameters were suited to fit this study: 100% infill density, utilization of a square printing pattern, alignment along the 0° flat axis, and adherence to a flat 0° printing angle.

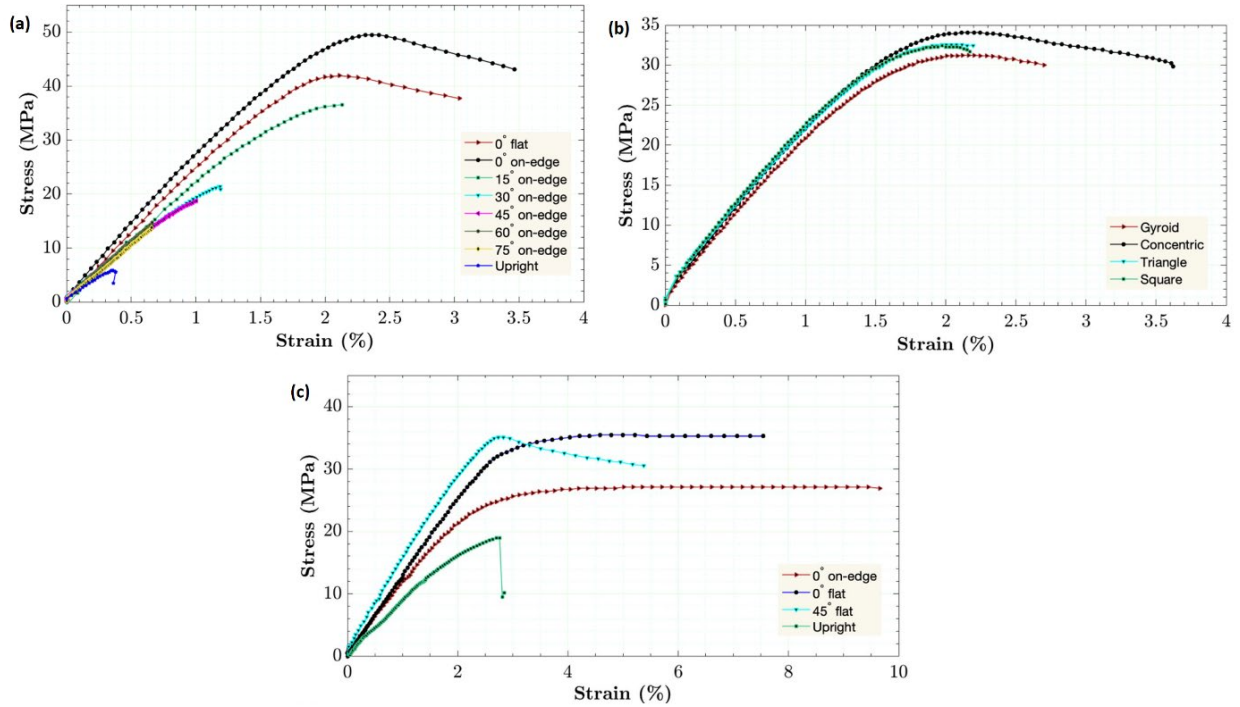


Figure 4. Stress-strain curves of the effect of printing angle (a), pattern (b) and axis (c) on tensile strength [16].

When designing solid parts, the FoS must be taken into consideration. By applying the FoS, any uncertainty in new designs is eliminated. Including this coefficient is crucial for developing a design that ensures safety and durability over an extended period. The FoS can be determined based on the purpose of the design, as well as the anticipated environmental conditions and expected period of use. The calculation of this coefficient is typically performed as follows [17]:

$$\sigma_{allow} = \frac{S_y}{N_{design}} \quad (5)$$

In this context, ' σ_{allow} ' stands for the safe stress limit, ' S_y ' for the failure stress, and ' N_{design} ' for the design factor [17].

Table 1. General FoS according to load types [16].

Load Types	Factor of Safety
Static short-term loads	1-2.5
Static long-term loads	2-5
Varying loads	4-10
Repetitive loads	5-15
Fatigue loads	5-15
Impact loads	10-15

Table 1 shows that materials with a factor of safety below '1' fail and break. Furthermore, the factor of safety must be at least '2' to ensure a durable design [17].

This study aims to reduce the amount of material utilized in 3D-printers. In this regard, a shelf bracket was developed, and its weight was reduced by applying topology optimization, resulting in a 70% material savings. Following that, these brackets were then subjected to a series of experiments, which verified the results of the analyses. The most significant innovation of the study that should be highlighted is that it gives an example framework that is simple to follow. The experimental setup requires no industrial equipment and can be carried out in any workshop. Furthermore, this study could be replicated in a wide range of disciplines, from industrial applications to other experimental setups.

2. RELATED LITERATURE

Within the existing body of literature, numerous studies have been conducted to attain enhanced lightness to optimize material usage with many research goals in mind.

Özsoy et al. [18] conducted a study where they performed mass optimization on an N95-type mask to save material for 3D-printing. Initially weighing 66.27 g, the mask underwent optimization, reducing by 30%, 40%, and 50% in weight. A decrease in weight was successfully accomplished, resulting in the conservation of material.

In the study carried out by Çelebi and Tosun [19], a mass optimization of 63% was applied to the samples. Subsequently, the optimized parts were manufactured with an FDM printer, and the unoptimized parts were produced via a CNC Router. Then, their mechanical properties were tested, and the results were compared. Consequently, the machined parts turned out to be stronger.

The study's objective conducted by Korkut and Koçak [20] was to investigate the potential reduction in the mass of an unmanned aerial vehicle's nose landing gear fork by utilizing TO. Based on the findings reported in the study, it was observed that a saving of 20-30 g of fuel per 100 km can be achieved for every 1 kg of weight reduced in the aircraft. When this fuel saving is multiplied by the annual flight time, it was found that 1 kg of weight reduction may save more than 2 million kg of fuel in a year. This optimization process reduced the part's mass from 2.54 kg to 1.51 kg while maintaining rigidity at a comparable level.

Aslan's study [6] aimed to achieve optimal geometry in a suspension swing arm by utilizing TO and lattice structural optimization techniques. The optimization outcomes were compared by employing three distinct lattice types. The initial mass of the object was 1.403 kg. Subsequently, it underwent a series of reductions, resulting in masses of 1.260 kg, 1.28487 kg, 1.31050 kg, and 1.249988 kg, respectively. The initial stress level was recorded as 252 MPa, followed by subsequent 184, 291, 287, and 317 MPa measurements. Consequently, the outcome of the third category of lattice optimization yielded the most desirable solution.

Top et al. [21] conducted a technical analysis of the bracket associated with the handbrake mechanism to be produced with AM techniques. A force of 500 N was exerted on the fastening holes of the brake mechanism in the model, resulting in a 43% reduction in the final mass of the formed shape, which measured 1.272 kg.

The study carried out by Demir et al. [22] aimed to apply topology optimization on a mobile transportation robot's chassis to reduce its weight by 20%. According to their findings, after the topology optimization application, the maximum stress value was found to be 48 MPa, and a value of 5.7 for the factor of safety. In conclusion, Demir et al. achieved a lighter design while maintaining structural rigidity.

3. MATERIALS AND METHOD

As seen in Fig. 5, small and large-scale models with dimensions of 90-90 mm and 155-135 mm were designed to conduct two different experiments. The choice was made with the purpose of breaking one bracket within the test setup because the analysis results indicated that the large-scale bracket would not fail when subjected to the maximum load with the testing equipment.

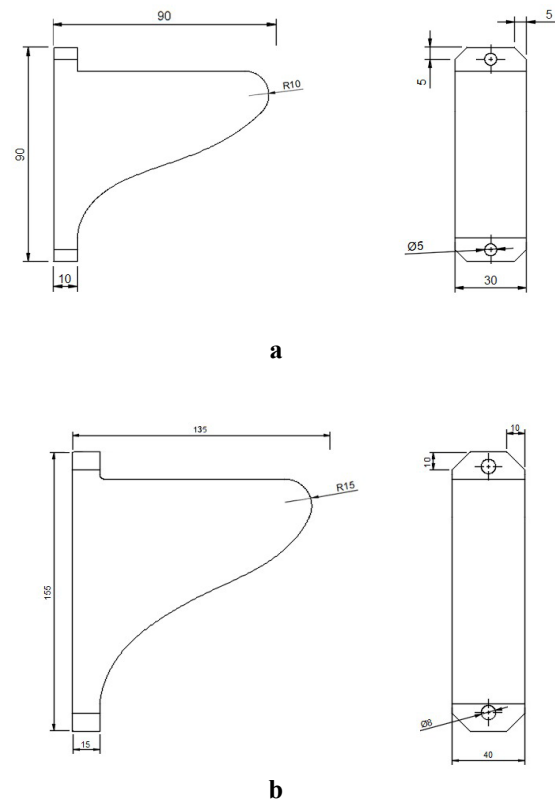


Figure 5. The technical drawings of the two brackets, Fig. 5-a depicting the 90-90 mm (small) bracket and Fig. 5-b the 155-135 mm (large) bracket.

These brackets have been subjected to a short-term static load in this study. The testing equipment at hand and the designed bracket geometry were best suited for this type of load. Therefore, dynamic loads were not investigated in this study.

Then, two designs were created accordingly. Following the design of the large and small brackets, initial mass and volume optimization experiments were conducted using ANSYS. The element dimension was originally set to 2 mm. However, due to the intricate nature of the surface, resulting from the application of TO, the reanalysis of the optimized geometry to validate the findings encountered mesh quality errors. In order to address this issue, the size of the element was reduced to 1 mm and 0.5 mm respectively. However, the intricacy of the problem proved to be formidable, to the extent that even a computer with moderate specifications, equipped with 16 GB of RAM, could not resolve it. The small bracket contained as many as 500,000 elements, and it couldn't be resolved.

Because of the unresolved issue, a decision was made to migrate to Autodesk Fusion 360. Due to its web-based nature, Fusion 360 operates on cloud infrastructure. Consequently, it does not impose any computational burden on the local machine.

Later, these models were imported into Fusion 360 for analysis. Subsequently, a mesh assignment was allocated to these components. The mesh quality was defined as 2 mm. Then, the load and the fixation of the holes were set as boundary conditions. Next, the structural analysis was commenced. The obtained results later get sent to the module for shape optimization. This process identifies and excludes critical regions by assigning appropriate boundary conditions. These critical regions refer to areas with holes and locations where the bracket will contact the wall. Additionally, the mass reduction technique eliminates regions with no significant impact on the component's overall strength and natural frequency. Afterward, the redundant regions were modeled and eliminated by projecting the formed structures onto the main component.

Performing smoothing after the completion of topological optimization in Fusion 360 is not recommended due to the additional removal of material from an already optimized structure, which may adversely impact its mechanical properties.

Following the completion of the design phase, two samples were fabricated utilizing PLA as the material in the process of 3D-printing. The samples consisted of one small-sized and one large-sized prototype.

According to Dhinesh et. al. [23] studies' test results, polylactic acid (PLA) showed better tensile strength and less deformation than acrylonitrile butadiene styrene (ABS). Due to this rationale, the selection of PLA material was made.

The mechanical and temperature properties of the PLA used in this study may be seen in the table below:

Table 2. Characteristics of the PLA used [24, 25]

Properties	Unit	Value
Density	kg/m^3	1,28
Tensile Strength	MPa	62,9
Yield Strength	MPa	56
Young Modulus	MPa	2850
Shear Modulus	MPa	1070,6
Poisson Ratio		0,33
Charpy Impact	kJ/m^2	14,2
Nozzle Temperature	$^{\circ}C$	200-230
Bed Temperature	$^{\circ}C$	60-75

The average value of the Poisson ratio for PLA was taken from the study of Ferreira et al [26].

The 90-90 mm prototype underwent a testing procedure resulting in its failure at a load of 2000 N. According to the simulation results the bracket was supposed to fail at a load of 1200 N. This corresponds to an error rate of 66.6%.

As for the bracket with 155-135 mm dimensions, it experienced failure when subjected to a force of 1000 N. The yield strength determined from the analysis was determined to be 3400 N. This discrepancy represents a 240% margin of error, which is highly implausible in practical terms.

Upon examination of the internal structure of the fractured brackets, it becomes evident that a hollow structure is present. A part manufactured at a 100% infill rate must exhibit a complete absence of voids within its internal structure. The potential causes of this error may include inaccuracies in the printing parameters or obstructions within the extruder nozzle.

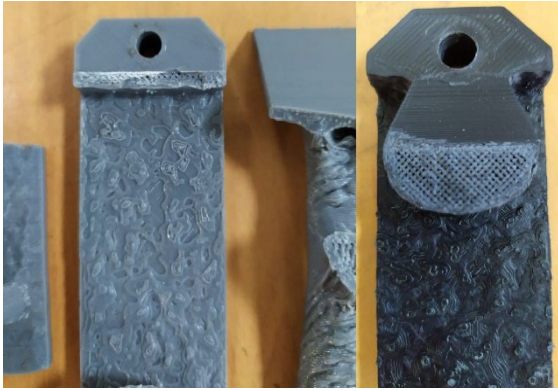


Figure 6. The brackets' internal structure.

As seen in Fig. 6, this is a defective part since the brackets didn't fail from its determined area. The hollow structures may be seen in Fig. 6. These gaps are minor in the smaller bracket. In the case of the large bracket, because it is larger in size, the dimensions of the air gaps have proportionately enlarged, resulting in a considerable drop in strength beyond what the simulation indicated.

This behavior may be attributed to infill density. The failure of the 3D-printing machine to reach a complete infill rate led to the production of a flawed bracket. According to Gonabadi et. al. [16], the strength of PLA parts will decrease as the infill rate decreases.

3.1. Different Solution Suggestions

It is crucial to thoroughly examine the nozzle of the 3D-printing machine to identify and address any potential issues related to clogging.

When setting up the testing equipment, it is important to ensure the accurate application of the load. Otherwise, an inaccurate measurement may be obtained, and the magnitude of the load may vary depending on the location of the rope suspension.



Figure 7. Failure resulting from incorrect placement of the load.

As shown in Fig. 7., failure under a larger load than expected by the analysis may be attributed to a misplacement of the rope's suspension point, resulting in the application of force from an inappropriate location.

4. ANALYSIS RESULTS

The static structural analysis and the optimization results are presented in this section. Refer to Fig. 8 for the related pictures.

Firstly, the 90-90 mm bracket was subjected to a load of 1200 N, and then the deformation, von Mises stress, and FoS value were determined. Subsequently, a 70% reduction in mass was applied to the bracket to optimize it. Next, an additional static structural analysis was conducted on the optimized bracket to validate the findings and establish a comparative analysis with the previous outcomes.

As seen in Fig. 8-a., in the unoptimized configuration of the 90-90 mm bracket, the observed maximum deformation was determined to be 0.3481 mm at the tip of the bracket. At the same time, the mass of the component was measured to be 149 grams.

Regarding the von Mises stress, it came out to be 38.31 MPa. Fig. 8-b shows the areas around the holes with the largest stresses, with the bottom hole having the highest strains.

As shown in Fig. 8-c, the unoptimized 90-90 mm bracket exhibited a FoS of 1.6419 when subjected to a load of 1200 N. Consequently, it can be deemed suitable for long-term load applications at values below 1200 N.

As shown in Fig. 8-d, the mass has lowered from 149 grams to 46 grams following optimization. The optimized bracket was then subjected to another static structural analysis to confirm the findings.

In the post-optimization design, the maximum von Mises stress around the bottom hole increased from 38.31 MPa to 56.45 MPa, which may be seen in Fig. 8-e. This is a 47.35% increase in stress. To confirm whether the design will fail or not, the FoS was checked.

Based on the data presented in Fig. 8-f, the FoS for the lower hole is 0.9921. The FoS experienced a decrease of 60.44%. Given that the value is below '1', the bracket will yield under this load magnitude. It is advisable to apply values that are below 1200 N for this small bracket. Next, the magnitude of the load was halved to achieve a better FoS value.

After decreasing the load to 600 N, an increase of 99.98% was observed in the FoS: As seen in Fig. 8-g, it came out to be 1.984. This design is deemed safe under this load magnitude and may be used for long-term applications.

Next, the 155-135 mm bracket analysis was held. A load of 3400 N was applied to the bracket. Then the deformation, von Mises stress, and the FoS values were determined.

As shown in Fig. 8-h, the maximum deformation was determined to be 0.5123 mm at the tip of the bracket.

In Fig. 8-i, the max. von Mises stress occurs at the bottom hole with a value of 52.18 MPa.

In Fig. 8-j, the safety factor of the bracket was determined to be 1.205, so no yielding will be observed. However, using it with loads lower than 3400 N is recommended to be safe.

Subsequently, the mass of the bracket was reduced by 70%, and it was subjected to another static structural analysis to confirm these results. The weight of the 155-135 mm bracket was decreased to 154 grams after 70% mass optimization.

As depicted in Fig. 8-k, the maximum von Mises stress was observed to be 63.24 MPa at the bottom hole. This means a 21.2% MPa increase in von Mises stress over the non-optimized result.

As seen in Fig. 8-l, the 155-135 mm bracket exhibits yielding due to optimization, as indicated by a FoS of 0.8499. The FoS experienced a decrease of 41.78% when compared to the non-optimized bracket. Then, the load's magnitude was reduced by 50% to attain a FoS value surpassing 0.8499.

As shown in Fig 9-m, the FoS in the lower hole increased by 208% to 1.7678 when the load was reduced. It may be used safely under long-term loads without yielding under this load.

The table below contains all the analysis results of the 90-90 mm bracket.

Table 3. 90-90 mm bracket's analysis data.

Bracket	Deformation (mm)	Stress (MPa)	FoS	Mass (g)
90-90 mm optimize d (600 N)	0,407	28,2 2	1,984	46
90-90 mm optimize d (1200 N)	-	56,4 5	0,992 1	46
90-90 mm (1200N)	0,3841	38,3 1	1,641 9	149

It can be seen from Table 3 that there is no deformation data of the optimized bracket under a load of 1200 N. The inclusion of this data is unnecessary as the brackets in question are expected to fail regardless.

The rest of the analysis results are shown in Table 4.

Table 4. 155-135 mm bracket's analysis data.

Bracket	Deformation (mm)	Stress (MPa)	FoS	Mass (g)
155-135 mm optimized (1800 N)	0,6381	35,58	1,767 8	154
155-135 mm optimized (3400 N)	-	63,24	0,849 9	154
155-135 mm (3400 N)	0,5123	52,18	1,205	512

As in Table 3, the deformation data here is not needed.

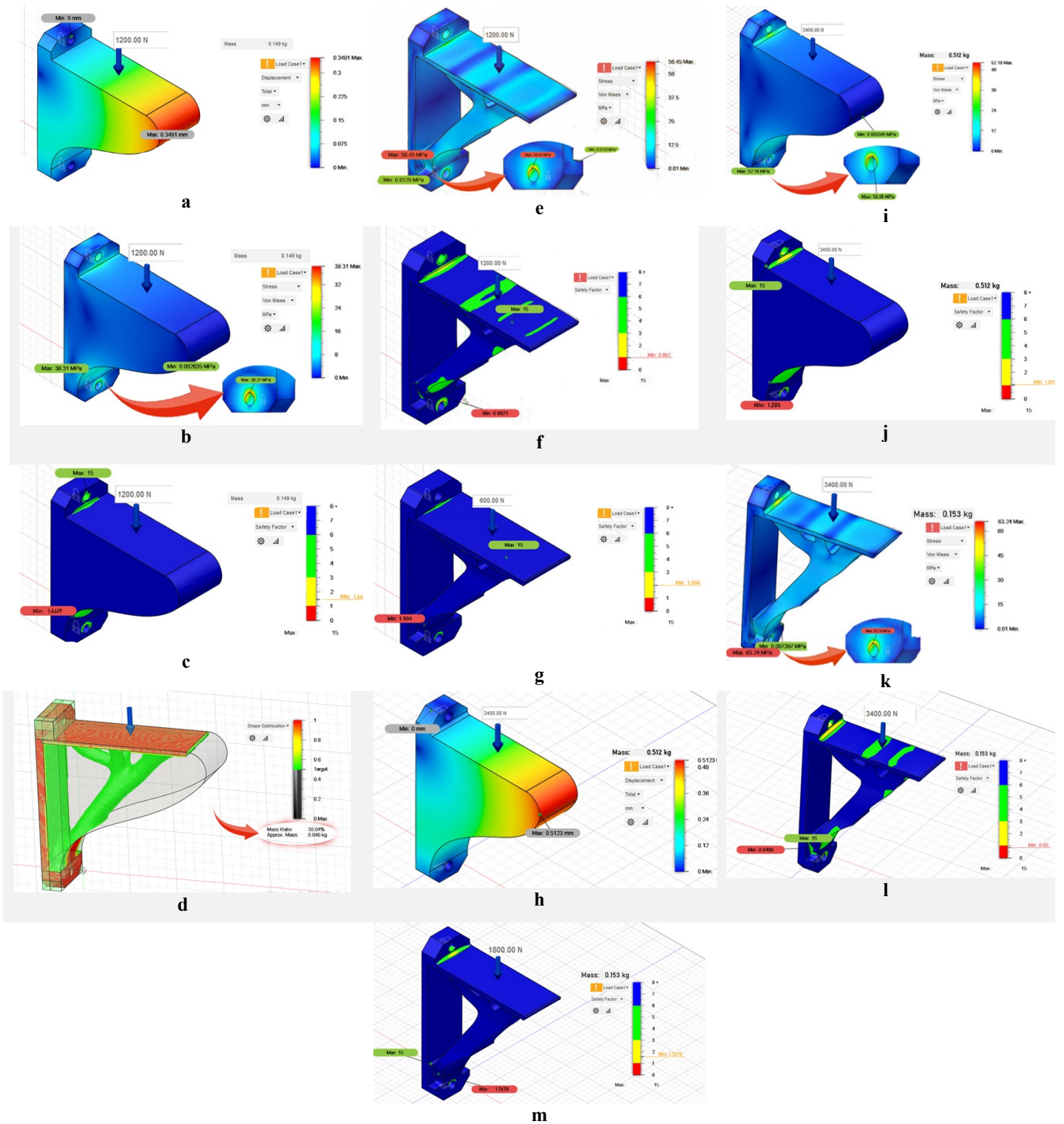


Figure 8. The analyses results for both brackets, **a)** The deformation of the 90-90 mm bracket. **b)** The von Mises stress of the 90-90 mm bracket. **c)** The FoS of the 90-90 mm bracket. **d)** The geometric shape resulted from a 70% reduction in mass through the implementation of topology optimization. **e)** The von Mises stress of the 90-90 mm bracket after optimization. **f)** The FoS of the 90-90 mm bracket after optimization. **g)** The FoS of the optimized 90-90 mm bracket under 600 N load. **h)** The deformation of the 155-135 mm bracket. **i)** The von Mises stress of the 155-135 mm bracket. **j)** The FoS of the 155-135 mm bracket. **k)** The von Mises stress of the 155-135 mm bracket after optimization. **l)** The FoS of the 155-135 mm bracket after optimization. **m)** The FoS of the optimized 155-135 mm bracket under 1800 N load.

5. EXPERIMENTAL RESULTS

After completing the analyses and optimizations for both brackets, the obtained results were converted into STL format and imported into Prusa Slicer. During the slicing phase, the layer thickness was determined to be 0.1 mm, the infill rate was set to 100%, and lines printing pattern was selected for the internal structure. The nozzle temperature was 210°C, while the bed temperature was set to 60°C. In this study, Porima's PLA filament [27] was used for the printing material. Under these conditions, printing for the smaller bracket took 4.5 hours, and for the larger one, it took 20.

Once the manufacturing process was finished, then the test setup was established. First, a hole was drilled in a steel workbench. This was done to ensure that there is no deformation at the connection points when a load is exerted on these brackets. Only the bracket should be exposed to deformation. Therefore, only the bracket itself is affected when there is yielding. To mitigate potential damage to the holes in the bracket caused by screw heads, a washer is placed between them to facilitate a more uniform distribution of the load. The side view of the connection mechanism of the larger bracket may be seen in Fig. 9.



Figure 9. The connecting mechanism of the 155-135 mm bracket.

A wooden wedge was inserted between the rope, which was fastened to the upper part of the bracket, and its flat surface to achieve a more uniform distribution of the load on the bracket. Subsequently, the rope was threaded underneath the wedge and suspended from the

digital scale, as depicted in Fig. 10. The digital scale used has a maximum load capacity of 300 kg or 3000 N.

A long iron bar was attached using a bolt on the workstation and utilized as a lever to make the application of force more regulated. To keep the travel of the lever short, the length of the rope was kept short as well. To facilitate the lever's movement, avoiding excessive tightening of the nut that secures it to the workbench is advisable.



Figure 10. The load that the 90-90 mm bracket (a) fails at, and the 155-135 mm bracket withstands (right), the test setup for the experiment (b).

The experimental procedure involved capturing footage using a camera with a frame rate of 60 frames per second (FPS). Subsequently, a screenshot was extracted from the video editing software, specifically when the ultimate yield occurred. The magnitude of the

yielding in the smaller bracket was measured to be 1213.5 N, which may be seen in Fig. 10.

Upon examination, a discrepancy of 1.125% was found of the failure forces between the experimental and analytical findings for the 90-90 mm bracket. This difference in forces is quite marginal. However, this may be attributed to the limitations of the analysis software, which cannot simultaneously discern transverse isotropic and orthotropic structures, also known as 3D-printed materials. Furthermore, during the process of manufacture, the filament may not always adhere properly, resulting in poor strength. In addition, the digital scale may also suffer losses, and the slack or flex in the rope may all contribute to this disparity.

Ultimately, the large bracket overloaded the scale, enduring a load of 3000 N without any signs of yielding. This means that the large bracket is significantly stronger than the small one.

According to Bell and Siegmund [30], the strength of 3D-printed components increases as their size grows. Experimenting with small and large specimens, they determined that larger specimens would fail at higher stresses. This is attributed to the size of the layer thickness. As the size of the layer thickness increases, its' strength will increase as well.

6. COST ANALYSIS

Based on the data provided by Porima [27], the cost of 1 kg of PLA filament is 15.08 USD. This amounts to 0.01508 USD per gram. So, the cost of filament utilized in this study may be determined by multiplying the filament quantity and its unit cost:

$$C = n * m * g \quad (6)$$

Here 'C' equates to the total cost to manufacture one bracket. 'n' represents the number of brackets to be manufactured, 'm' represents the total mass of filament used, and 'g' denotes the cost of filament per gram.

The combined cost of a 90-90 mm and a 155-135 mm bracket equals just over 3 USD.

According to this cost analysis, mass optimization has resulted in a 70% reduction in the production cost of these shelf brackets.

7. CONCLUSION

This study demonstrates the feasibility of improving lightness and rigidity while achieving material savings through various optimization techniques. There has been a logical trend toward producing complex structures utilizing multiple materials and AM techniques in recent years.

A significant reduction of 70% in mass has been successfully achieved, resulting in the development of a safe design capable of withstanding loads below 3000 N. When comparing the findings of this study to the study conducted by Yıldız [28], it can be observed that the application of TO was more effective in our study. In Yıldız's study, applying TO reduce the weight of the control arm by 13.5%, meanwhile increasing the maximum stress by 24.16%. The findings of our study indicate that there was a modest 17.5% increase in maximum stress when comparing the optimized and unoptimized 155-135 mm brackets while reducing their mass significantly.

Based on this study's empirical and theoretical evidence, the idea suggesting the feasibility of concurrently generating light and highly rigid components through topology optimization has been proven.

This study could be more precisely replicated using alternative test equipment. Better precision may be achieved by designing a specimen specifically engineered for experimentation within a hydraulic press. Additionally, ANSYS may potentially be used to examine dynamic loads with a simpler design. Then this part may be tested using an axial accelerometer to confirm the analysis findings [29].

Consistent with the project's objectives, the analytical and experimental processes effectively demonstrated material conservation, lightweight construction, and structural rigidity. By carefully considering the design options and criteria outlined in the study and considering alternative solution proposals, this research may be replicated and expanded upon by employing different topology and production techniques.

ACKNOWLEDGES

This study was carried out in the Istanbul Gedik University Vocational School 3D printing lab and the machine workshop with the assistance of Research Assistant Emre Tuğberk GÜLNERGİZ and Technician Ismail ÖRS.

REFERENCES

- Liu, S., Li, Q., Liu, J., Chen, W., Zhang, Y., "A Realization Method for Transforming a Topology Optimization Design into Additive Manufacturing Structures", *Engineering*, Vol. 4, Issue 2, Pages 277-285, 2018.
- Brackett, D., Ashcroft, I., Hague, R., "Topology Optimization for Additive Manufacturing", *International Solid Freeform Fabrication Symposium*, 348-362, Austin, Texas, 2011.
- Moaveni, S., "Finite Element Analysis: Theory and Applications with ANSYS 4th Edition", Pages 2-8, Pearson, USA, 2014.
- MacNeal, R. H., "Some Organizational Aspects of NASTRAN", *Nuclear Engineering and Design*, Vol. 29, Issue 2, Pages 254-265, 1974.
- Ergin, A., Bayraktarkatal, E., Ünsan, Y., "Sonlu Elemanlar Metodu ve Gemi İnşaatı Sektöründeki Uygulamaları", *Türk Loydu Vakfı*, 1-3, İstanbul, 2000.
- Aslan, B., "Yenilikçi Tasarım Yöntemleri Kullanarak Eklemeli İmalata Yönelik Optimum Ürün Geliştirilmesi", *Yüksek Lisans Tezi*, Bursa Teknik Üniversitesi, Bursa, 2019.
- Vlah, D., Žavbi, R., Vukašinović, N., "Evaluations of Topology Optimization and Generative Design Tools as Support for Conceptual Design", *International Design Conference*, Pages 451-460, Cambridge, 2020.
- Ege, M., Küçük, S., "Energy Minimization of New Robotic-Type Above-Knee Prosthesis for Higher Battery Lifetime", *Applied Sciences*, Vol. 13, Issue 6, Pages 3868, 2023.
- Larsson, J., Wennhage, P., Göransson, P., "Mass Minimization with Conflicting Dynamic Constraints by Topology Optimization Using Sequential Integer Programming", *Finite Elements in Analysis and Design*, Vol. 200, Pages 1-10, 2022.
- Aktimur, B., Gökpınar, E., "Katmanlı Üretim Havaçılıktaki Uygulamaları", *Gazi University Journal of Science Part C: Design and Technology*, Vol. 3, Issue 2, Pages 463-469, 2015.
- Turhan, S., Özsoy, A., "DLMS Yöntemiyle İmal Edilen Ti6Al4V Alaşım Özelliklerine İşlem Parametrelerinin Etkisi", *Uluslararası Teknolojik Bilimler Dergisi*, Vol. 8, Issue 2, Pages 15-27, 2016.
- Frazier, W. E., "Metal Additive Manufacturing: A Review", *Journal of Materials Engineering and Performance*, Vol. 23, Pages 1917-1928, 2014.
- Wohlers, T., Gornet, T., "History of Additive Manufacturing", *Wohlers Report*, Wohlers Associates, 2015.
- Sidambe, A. T., "Biocompatibility of Advanced Manufactured Titanium Implants—A Review", *Materials*, Vol. 7, Issue 12, Pages 8168-8188, 2014.
- Hanon, M. M., Marczis, R., Zsidai, L., "Influence of the 3D Printing Process Settings on Tensile Strength of PLA and HT-PLA", *Periodica Polytechnica Mechanical Engineering*, Vol. 65, Issue 1, Pages 38-46, 2021.
- Gonabadi, H., Yadav, A., Bull, S. J., "The Effect of Processing Parameters on the Mechanical Characteristics of PLA Produced by a 3D FFF Printer", *The International Journal of Advanced Manufacturing Technology*, Vol. 111, Issue 3-4, Pages 695-709, 2020.
- Hibbeler, R. C., "Mechanics of Materials 8th Edition", Pages 46-48, Pearson, USA, 2010.
- Özsoy, K., Şentürk, E., Aydoğan, D., Korucu, Ö. E., "3B Yazıcı Teknolojisi için Topoloji Optimizasyonu: N95 Maske Üzerine Bir Çalışma", *Türk Doğa ve Fen Dergisi*, Vol. 9, Pages 152-159, 2020.
- Çelebi, A., Tosun, H., "Application and Comparison of Topology Optimization for Additive Manufacturing and Machining Methods", *International Journal of 3D Printing Technologies and Digital Industry*, Vol. 5, Issue 3, Pages 676-691, 2021.
- Koçak, M. R., Korkut, İ., "İnsansız Hava Aracı Burun İniş Takımı Çatalı için Topoloji Optimizasyonu Uygulaması", *Politeknik Dergisi*, 1-1, 2022.

21. Top, N., Gökçe, H., Şahin, İ., “Eklemeli İmalat İçin Topoloji Optimizasyonu: El Freni Mekanizması Uygulaması”, Journal of Selcuk-Technic, Vol. 18, Issue 1, Pages 1-13, 2019.
22. Demir, N., Sucuoğlu, H. S., Böğrekci, İ., Demircioğlu, P., “Topology Optimization of Mobile Transportation Robot”, International Journal of 3D Printing Technologies and Digital Industry, Vol. 5, Issue 2, Pages 210-219, 2021.
23. Dhinesh, S. K., Arun Prakash, S., Senthil Kumar, K. L., Megalingam, A., “Study on Flexural and Tensile Behavior of PLA, ABS and PLA-ABS Materials”, Materials Today: Proceedings, Vol. 45, Pages 1175-1180, 2021.
24. Porima 3D, “Porima PLA Filamentler”, <https://static.ticimax.cloud/42373/uploads/dosyalar/porima-tds-tr.pdf>, January 13, 2023.
25. Porima 3D, “Porima PLA Filamentler”, <https://static.ticimax.cloud/42373/Uploads/Dosyalar/porima3d-e-katalog.pdf>, January 13, 2023.
26. Ferreira, R., Amatte, I. C., Dutra, T. A., Bürger, D., “Experimental Characterization and Micrography of 3D Printed PLA and PLA Reinforced with Short Carbon Fibers, Composites”, Part B Engineering, Vol. 124, Issue 1, Pages 88-100, 2017.
27. Porima 3D, “Porima PLA Filamentler”, <https://www.porima3d.com/porima-pla-filament>, January 13, 2023.
28. Yıldız, A. R., “Taşıt Elemanlarının Yapısal Optimizasyon Teknikleri ile Optimum Tasarımı”, Politeknik Dergisi, Vol. 20, Issue 2, Pages 319-323, 2017.
29. Çağlayan, B. Ö., Ozakgöl, K., Tezer, Ö., “Assessment of a Concrete Arch Bridge Using Static and Dynamic Load Tests”, Structural Engineering and Mechanics, Vol. 41, Issue 1, Pages 83-94, 2012.
30. Bell, D., Siegmund, T., “3D-printed polymers exhibit a strength size effect”, Additive Manufacturing, Vol. 21, Issue 1, Pages 658-665, 2018.